Chinese Chemical Letters 34 (2023) 107337

Contents lists available at ScienceDirect

Chinese Chemical Letters

journal homepage: www.elsevier.com/locate/cclet

W/Mo-polyoxometalate-derived electrocatalyst for high-efficiency nitrogen fixation

Hua-Qing Yin[1], Lu-Lu Yang[1], Hao Sun, Hao Wang, Yu-Jie Wang, Min Zhang, Tong-Bu Lu, Zhi-Ming Zhang*

Institute for New Energy Materials & Low Carbon Technologies, School of Materials Science and Engineering, Tianjin University of Technology, Tianjin 300384, China

ARTICLE INFO

Article history:
Received 16 February 2022
Revised 7 March 2022
Accepted 15 March 2022
Available online 17 March 2022

Keywords:
Polyoxometalate
Electrocatalysis
Mixed-metal electrocatalyst
Nitrogen reduction
Mild conditions

ABSTRACT

Ammonia is the feedstock chemical for most fertilizers and the alternative of renewable energy carriers. Environmentally benign electrochemical nitrogen reduction reaction (NRR) under mild conditions has been recognized as one of the most attractive strategies for N_2 fixation. Herein, inspired by Mo-based nitrogenase, W/Mo-doping electrocatalysts were developed with mixed-metal polyoxometalate $H_3PW_6Mo_6O_{40}$ as the precursor for high performance electrocatalytic NRR. Trace amount of Pt was transplanted on the surface of W/Mo@rGO *via in situ* electroplating treatment to further improve the NRR performance. The resulting Pt-W/Mo@rGO-6 achieves excellent performance for NRR with a high NH_3 yield of 79.2 μg h^{-1} mg_{cat}^{-1} due to the multicomponent synergistic effect in the composite catalyst. The Pt-W/Mo@rGO-6 represents the first example of highly efficient NRR electraocatalyst derived from mixed-metal polyoxometalate, which exhibits outstanding stability confirmed by the constant catalytic performance over 24 h chronoamperometric test. This finding opens a new avenue to construct highly efficient NRR electrocatalyst by employing mixed metal polyoxometalate as the precursor under ambient conditions.

Ammonia (NH_3), as an important feedstock chemical, is indispensable in manufacturing agricultural fertilizers, industry extensively products, and carbon-free condensed fuels [1,2]. As well known, biological ammonia synthesis can only support a fraction of today's global NH_3 requirement [3]. Since the nitrogen reduction reaction (NRR) catalyst emerged in 1807, the Haber–Bosch method has been regarded as one of the most important strategies for N_2 fixation [4–7]. However, the Haber-Bosch N_2 fixation process has to be performed under high pressure and high temperature (around 400 °C, 15-25 MPa), which usually suffers from severe equipment requirements and causes serious environmental issues [8–11]. Although N_2 is abundant in the atmosphere, NRR has proven to be extremely challenging under mild conditions due to its high bond energy of N≡N (940 kJ/mol) and non-polarizable N_2 molecule [12–15]. It is highly attractive to explore alternative strategies for N_2 fixation under mild conditions for sustainable energy solutions [16–21].

Up to date, high-performance NRR catalysts mostly depend on noble metals (Pt, Pd, Au, Ru, *etc.*) and lanthanide ions [22,23]. In this filed, Yang *et al.* combined Au and nanoporous hydrophobicity zeolitic imidazole framework (ZIF) as NPG@ZIF-8 to achieve a NH_3 yield of 28.7 mg h^{-1} cm^{-2} [24]. Ling and coworkers developed a Pt/Au electrocatalyst modified by ZIF, which shows satisfactory Faradaic efficiency (FE) of 44% and NH_3 yield of 161.9 μmol mg_{cat}^{-1} h^{-1} [25]. Meanwhile, Zhao and co-workers introduced Pb into Pd nanosponges to promote the adsorption of N_2, resulting a NH_3 yield of 25.68 μg mg_{cat}^{-1} h^{-1} with 5.79% FE [26]. However, the high cost and limited reserves of the noble metals seriously limit their large-scale application [27–29]. Recently, low-cost transition metals, such as Ti, Cu, Fe and Mn, have been used to construct NRR catalysts [30–33]. In this field, Ti^{3+} ion in Ti_2O_3 nanoparticles can be used as the active sites for promoting the NRR activity to achieve a NH_3 yield of 26.01 μg h^{-1} mg_{cat}^{-1} with a FE of 9.16% [31]. The Fe based C_{18}@Fe_3P/CP was also explored to activate the N_2 with a NRR performance of 2.16×10^{-11} mol s^{-1} cm^{-2} [33]. However, their NRR performance still need to be further improved to achieve satisfactory NH_3 yield. Therefore, it is necessary to innovate in the direction of high-performance, economical, and environmentally friendly nitrogen fixation strategies with high efficiency.

* Corresponding author.
E-mail address: zmzhang@email.tjut.edu.cn (Z.-M. Zhang).
[1] These authors contributed equally to this work.

https://doi.org/10.1016/j.cclet.2022.03.060
1001-8417/

Molybdenum (Mo) in nitrogenase has been recognized as the active center for N_2 fixation under mild conditions. In nitrogenases, Mo centers donate unpaired electron to antibonding orbitals of N_2 and accept lone electron pairs from N_2 to facilitate the dissociation of N≡N bonds [34–38]. Moreover, Mo located at the top of the NRR theoretical volcano plot, which induces Mo-based catalysts standing out from a series of metal catalysts for high-performance NRR electrocatalysts [39–42]. However, the reaction overpotential of Mo-based electrocatalysts are still higher than 0.5 V, leading to excessive energy consuming [43,44]. Recently, Du and co-workers reported that atomically dispersed tungsten (W) catalysts exhibited optimal performances for NRR with a low onset potential of 0.25 V according to the calculating theory and experimental results [45,46]. It is evidenced that Mo cooperates with W derivative to provide optimal adsorption of N_2 to improve NRR and impede the hydrogen evolution reaction [36]. Thus, it is reasonable to expect that heteronuclear W/Mo electrocatalysts would optimize the NRR activity and selectivity, which are not observable in their individual monometallic systems [47]. In this field, Liang and co-workers reported a Mo-PTA@CNT electrocatalyst by doping Mo into the phosphotungstic acid (PTA) [36]. In Mo-PTA@CNT, Mo and W display strong interaction with N_2 to achieve a high NH_3 yield rate of 51± 1 μg h^{-1} $mg_{cat}{}^{-1}$. Accordingly, it is expected that the W/Mo synergy in the uniformly dispersed dual-metal catalysts can maximize the atom utilization and improve the NRR activity. However, the synthesis of bimetal W/Mo-derived catalyst remains a huge challenge owing to the lack of uniform distribution and interaction techniques at an atom-level under the harsh synthesis condition. Hence, it is highly desirable to controllable synthesis of uniform-distributed W/Mo catalyst to provide in-depth insight into the synergetic mechanism for NRR. Polyoxometalates (POMs), with W/Mo-enriched structure and attractive electron/proton reservoir properties [48,49], are considered as excellent matrixes for construction of W/Mo derived co-catalysis.

Herein, we developed a W/Mo@rGO electrocatalyst *via* anchoring the heteronuclear $H_3PW_6Mo_6O_{40}$ (PW_6Mo_6) POM on reduced graphene oxide (rGO) following a calcining process. Further, trace amount of Pt was transplanted on the surface of W/Mo@rGO *via in situ* electroplating treatment as Pt-W/Mo@rGO-6 to further improve the performance for NRR at ambient conditions. It is noted that the W/Mo synergy effect obviously promotes the NRR efficiency with the NH_3 yield of 79.2 μg h^{-1} $mg_{cat}{}^{-1}$ at −0.3 V *vs.* RHE. The NRR performance of heteronuclear POM-derived Pt-W/Mo@rGO-6 was much superior to that of the catalysts derived from mono-metal POMs (Pt-W@rGO-6 and Pt-Mo@rGO-6). This work demonstrates POMs as efficient precursors for the construction of heterometallic composites to act as advanced NRR catalysts.

In nitrogenase, Mo centers can donate unpaired electron to antibonding orbitals of N_2 and accept lone electron pairs from N_2, which can facilitate the dissociation of N≡N bond. Accordingly, Mo doping represents an effective approach to supply catalytic active sites and modulate electronic structures to achieve N_2 fixation under mild conditions [50]. Inspired by nitrogenase, we selected Mo as the dopant to potentially lower the energy barrier of the dissociation of N≡N bond. The doped Mo species possess different d-electron structure from W, which allows tuning the electronic structure of W-based matrix for high efficient NRR [51,52]. In this work, PW_6Mo_6 was chosen and synthesized as the model POM for the construction of W/Mo catalyst. Powder X-ray diffraction (PXRD) illustrates the successful synthesis of PW_6Mo_6 (Fig. S1 in Supporting information). Then, according to the PXRD and Raman spectra, graphene oxide (GO) was produced successfully for further application (Fig. S2 in Supporting information) [53,54]. The detailed synthetic process of Pt-W/Mo@rGO-X electrocatalyst was schematically illustrated in Fig. 1. Firstly, a precursor solution was prepared

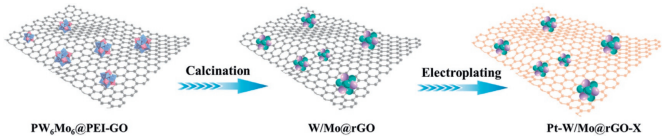

Fig. 1. Schematic synthesis of Pt-W/Mo@rGO-X (X means the electroplating time).

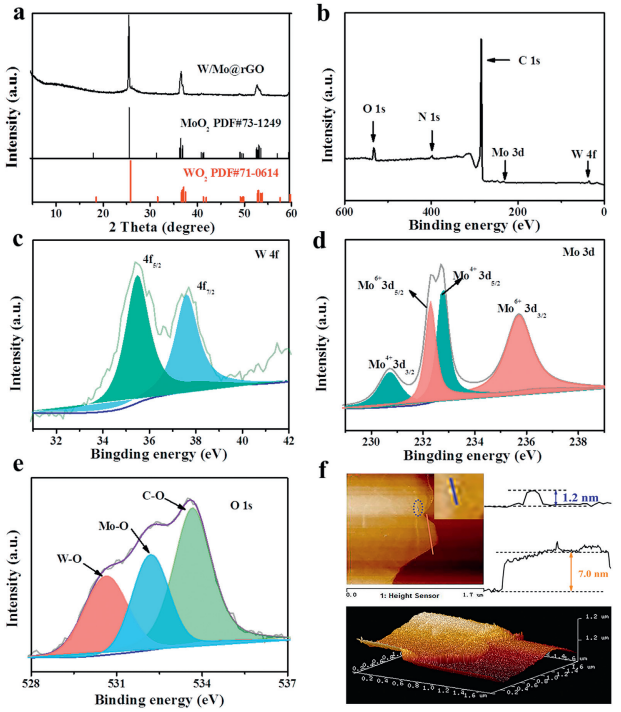

Fig. 2. (a) PXRD patterns of W/Mo@rGO and the simulated MoO_2 and WO_2. XPS spectra of (b) W/Mo@rGO, (c) W 4f, (d) Mo 3d and (e) O 1s. (f) AFM image of Pt-W/Mo@rGO-6.

by ultrasonic dissolution of PW_6Mo_6 in pure water in the presence of rGO. With the assistance of poly(ethylenimine) (PEI), PW_6Mo_6 was loaded onto the GO nanosheets to obtain PW_6Mo_6@PEI-GO. The PW_6Mo_6@PEI-GO precursor was then subjected to a calcining treatment to produce W/Mo oxide species on the surface of rGO to construct the W/Mo@rGO. To further improve the NRR catalytic activity, trace amount of Pt was electroplated for 6 h to form Pt-W/Mo@rGO-6. For comparison, the Mo-based Pt-Mo@rGO-6 and W-based Pt-W@rGO-6 electrocatalysts were further synthesized under the similar conditions.

The morphology and structure of Pt-W/Mo@rGO-6 were initially investigated by PXRD, high resolution transmission electron microscopy (HRTEM). As revealed in Fig. 2a, the XRD patterns of W/Mo@rGO displays characteristic signals located at 25.9° (110), 37.4° (002) and 53.5° (022), corresponding to characteristic peaks of WO_2 (PDF#71-0614) and MoO_2 (PDF#73-1249). TEM images reveal that W/Mo@rGO and rGO have the similar morphologies with obvious wrinkles, which illustrates unchangeable ultrathin rGO sheets before and after the fixation of W/Mo oxides (Figs. S3 and S4 in Supporting information). As shown in Fig. S4 in Supporting information, W/Mo oxide nanoparticles can be obviously observed on W/Mo@rGO with average particle size of *ca.* 31 nm (Fig. S4 in Supporting information). HRTEM image exhibits the ordered lattice fringes with a spacing of 2.4 Å, which corresponds to the (002) plane of WO_2 and the (200) plane of MoO_2. Further, energy dispersive X-ray (EDX) elemental mappings prove the uniform distribution of Mo and W elements on the rGO (Fig. S5 in Supporting information).

Further, X-ray photoelectron spectroscopy (XPS) was carried out to gain insight into the chemical states and components of W/Mo@rGO. As exhibited in Fig. 2b, XPS survey spectrum confirms the existence of W, Mo, N, O and C elements, which consists with the EDX elemental mapping results. As shown in Fig. 2c, the spin orbit split doublet W $4f_{7/2}$ and W $4f_{5/2}$ peaks were detected at 35.5 and 37.6 eV, which indicates the valence of W species between W^{4+} and W^{5+} [17,48]. Further, the Mo $3d_{5/2}$ and $3d_{3/2}$ peaks corresponding to Mo^{6+} in W/Mo@rGO can be observed at 232.2 and 235.7 eV; meanwhile the peak locations of 230.7 and 232.8 eV can confirm the existence of Mo^{4+} (Fig. 2d) [53]. It can be speculated that the surface oxidized Mo/W species impede further oxidation of WO_2 and MoO_2 in W/Mo@rGO, and the high valence W/Mo species can only be observed here by XPS because of its surface detection feature. To further demonstrate the reliability of the surface protection theory, the content of Mo^{6+} under Ar and atmosphere were detected *via* XPS spectra. There are approximate 52.4% Mo^{6+} on the surface of W/Mo@rGO under Ar, which was similar to that under atmosphere (54.0%) (Fig. 2d and Fig. S6a in Supporting information). Meanwhile, the spin orbit split doublet W $4f_{7/2}$ and W $4f_{5/2}$ peaks still locate at 35.5 and 37.6 eV without further oxidation under atmosphere (Fig. S6b in Supporting information). The WO_2 and MoO_2 in W/Mo@rGO observed in PXRD pattern can keep stable under atmosphere (Fig. S6c in Supporting information). All above results demonstrate the protection ability of the high valence W and Mo oxides on the surface of the catalysts to prevent the further oxidation of W^{4+} and Mo^{4+} inside the W/Mo@rGO. Hence, WO_2 and MoO_2 both exist in abundance in the W/Mo@rGO catalyst, which consists with the PXRD patterns. In the O 1s spectrum for W/Mo@rGO, the characteristic peaks at 530.5 eV and 532.1 eV belong to W-O and Mo-O, respectively (Fig. 2e). The C-O bond located at 533.6 eV is assigned to the characteristic peak of rGO [55]. In the Fourier transform infrared (FTIR) spectra of Pt-W/Mo@rGO-6, rGO and PW_6Mo_6, the characteristic peaks of PW_6Mo_6 located at 878.4, 976.4 and 1074.9 cm^{-1} disappeared in the FTIR spectra of Pt-W/Mo@rGO-6, which indicates the destruction of the POM (Fig. S7 in Supporting information) [56]. Atomic force microscopy of Pt-W/Mo@rGO-6 reveals that the average thickness of rGO nanosheets is around 7.0 nm to support about 1.2 nm W/Mo oxide nanoparticles (Fig. 2f).

After Pt electroplating, HRTEM images reveal that WO_2 and MoO_2 still keep the crystal lattice in Pt-W/Mo@rGO-6 with 3.4 Å lattice space, which corresponds to (110) facet of WO_2 and MoO_2 (Figs. 3a and b). Simultaneously, the HAADF-TEM image of Pt-W/Mo@rGO-6 clearly reveals the existence of WO_2 and MoO_2 nanoparticles anchored on rGO sheets (Fig. 3c). Further, the EDX elemental mapping exhibits the existence and uniform distribution of C, N, O, W, Mo and Pt in the composite catalyst of Pt-W/Mo@rGO-6 (Figs. 3d-i). The Pt content was determined to be 0.05 wt% *via* inductively coupled plasma mass spectrometry. The W and Mo contents on Pt-W/Mo@rGO-6 were determined to be 9.7% and 2.0%, respectively. As a comparison, Pt-W@rGO-6 and Pt-Mo@rGO-6 were synthesized with PW_{12} and PMo_{12} as the precusors, respectively, which were used as the control samples for further studying the NRR performance. From FTIR spectra, Mo or W oxide was successfully loaded on the rGO following a 6 h electroplating process to form Pt-W@rGO-6 and Pt-Mo@rGO-6 (Figs. S8 and S9 in Supporting information).

The NRR performance was determined at room temperature and atmospheric pressure with N_2-saturated electrolyte (0.05 mol/L H_2SO_4) in gas-tight two-compartment electrochemical cell. Firstly, linear sweeping voltammetry (LSV) curves were carried out to determine the electroplating time. As exhibited in Fig. 4a, the current density of Pt-W/Mo@rGO-6 enhances obviously comparing with that of W/Mo@rGO, Pt-W/Mo@rGO-2 and Pt-W/Mo@rGO-12. Hence, Pt-W/Mo@rGO-6 was chosen for further research of the

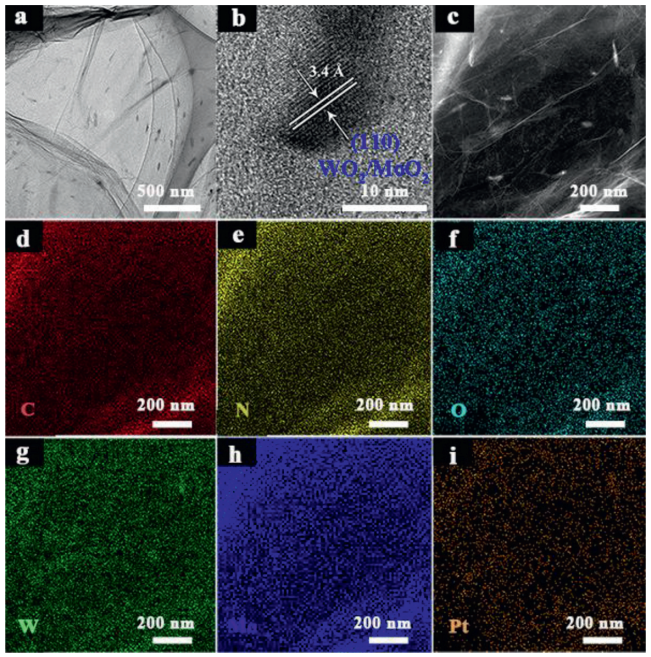

Fig. 3. (a) TEM, (b) HRTEM, (c) HADDF-TEM and (d-i) EDX elemental mapping images of Pt-W/Mo@rGO-6.

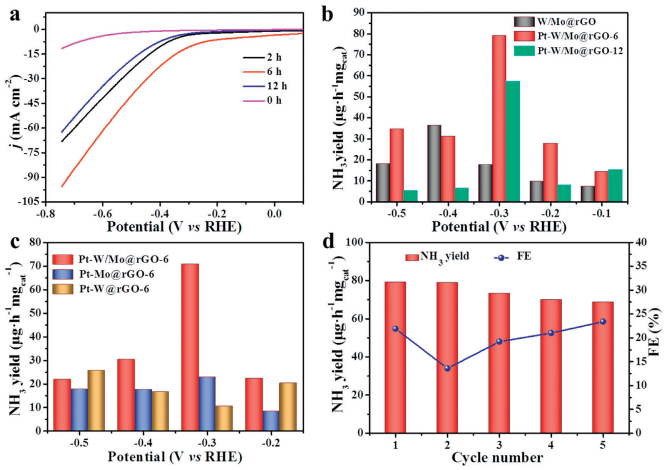

Fig. 4. (a) LSV curves of Pt-W/Mo@rGO-X (X = 2, 6, 12) with different electroplating time. (b) Corresponding NH_3 yields for W/Mo@rGO, Pt-W/Mo@r GO-6 and Pt-W/Mo@rGO-12. (c) The NH_3 yields of Pt-W/Mo@rGO-6, Pt-W@rGO-6 and Pt-Mo@rGO-6 under different electrolysis potentials. (d) Recycle experiments with Pt-W/Mo@rGO-6 as the catalyst at −0.30 V *vs.* RHE.

NRR efficiency in this work. As shown in Fig. S10 (Supporting information), the LSV curves were recorded from 0.2 V to −0.75 V with saturated N_2 or Ar, respectively. The current density in N_2 atmosphere was much higher than that in Ar atmosphere, especially for the potential exceeding −0.3 V, which indicates high activity of Pt-W/Mo@rGO-6 toward electrocatalytic NRR. The NH_3 yield enhenced with increasing the potentials from −0.1 V to −0.3 V with the maximum yield of 79.2 μg h^{-1} $mg_{cat}{}^{-1}$ at −0.3 V *vs.* RHE, which is 4 times higher than that of W/Mo@rGO (19.7 μg h^{-1} $mg_{cat}{}^{-1}$) (Fig. 4b, Figs. S11 and S12 in Supporting information). After 12 h electroplating, the NH_3 yield of Pt-W/Mo@rGO-12 decreased at −0.3 V *vs.* RHE (Fig. 4b) compared to that of Pt-W/Mo@rGO-6. With increasing the electrolysis potential from −0.1 V to −0.3 V, the current density and the yield of NH_3 increased significantly, however the NH_3 yield decreased significantly at

−0.4 V due to the competitive hydrogen evolution reaction in the aqueous solution.

Further, LSV curves of Pt-W/Mo@rGO-6, Pt-W@rGO-6 and Pt-Mo@rGO-6 were investigated to understand the synergy effect of Mo and W in depth and attest the superiority of Pt-W/Mo@rGO for promoting the NRR. As shown in Fig. S13 (Supporting information), the current density of Pt-W/Mo@rGO-6 from 0 to −0.7 V is much higher than that of Pt-W@rGO-6 and Pt-Mo@rGO-6. Notably, the NH_3 yield of Pt-W/Mo@rGO-6 was 7 and 3 times higher than that of Pt-W@rGO-6 and Pt-Mo@rGO-6, respectively. Additionally, the performance of Pt-Mo@rGO-6 was more than two times higher than that of the W-catalyst Pt-W@rGO-6. These results indicate the important role of Mo element in NRR and the fatal influence of Mo doping in improving the NRR performance (Fig. 4c). The outstanding performance of Pt-W/Mo@rGO is superior to that of most the state-of-the-art W/Mo-based catalysts (Table S1 in Supporting information).

Meanwhile, hydrazine as the possible by-product was detected by Watt and Chrisp method [57]. As shown in Fig. S14 (Supporting information), no obvious hydrazine can be detected in the NRR system, indicating a high selectivity of Pt-W/Mo@rGO-6 for the synthesis ammonia from N_2. After 24 h electrolysis, negligible attenuation of current density raised during NRR (Fig. S15 in Supporting information), and the NH_3 yield tended to be stable after five cycles of NRR at −0.3 V *vs*. RHE (Fig. 4d). The PXRD pattern of Pt-W/Mo@rGO-6 exhibits neglect signal change after five electrocatalytic cycles (Fig. S16 in Supporting information). All these results imply excellent stability of Pt-W/Mo@rGO-6 for electrocatalytic NRR. Additionally, a series of control experiments were carried out to confirm the reliable NRR detection. Firstly, no NH_3 can be observed in Ar-saturated solution rather than N_2-saturated electrolyte (Fig. S17a in Supporting information). Then, N_2 was used as a feedstock gas but under an open-circuit potential condition, where no NH_3 can be obtained (Fig. S17b in Supporting information). During the $^{15}N_2$-labeling experiments, ^{1}H NMR spectrum shows the doublet coupling signals of $^{15}NH_4^+$ (Fig. S18 in Supporting information). However, only triplet coupling signal for $^{14}NH_4^+$ can be detected with $^{14}N_2$ as feeding gas. All those results confirm N_2 as the N source of NH_3 rather than any nitrogenous species in catalyst or pollutants.

In conclusion, we have developed a highly efficient electrocatalyst Pt-W/Mo@rGO-6 with PW_6Mo_6 as the W/Mo precursor, which can promote NRR under mild conditions. In Pt-W/Mo@rGO-6, the synergetic effect of Mo and W species plays an important role on N_2 activation and dissociation for high efficiency NRR. Meanwhile, trace amount of electroplating Pt can further improve the performance of electrocatalytic NRR. The resulting Pt-W/Mo@rGO-6 catalyst shows a high NH_3 yield of 79.2 μg h^{-1} mg_{cat}^{-1} at a low potential of −0.3 V *vs*. RHE, which is superior to that of most the state-of-the-art W/Mo-based catalysts. This finding opens a new avenue to construct highly efficient NRR electrocatalyst by employing mixed-metal POMs as the precursors.

Declaration of competing interest

The authors declare that they have no known competing financial interests or personal relationships that could have appeared to influence the work reported in this paper.

Acknowledgments

This work was supported by the National Natural Science Foundation of China (Nos. 92161103, U21A20286, 22071180), Natural Science Foundation of Tianjin City of China (No. 18JCJQJC47700).

Supplementary materials

Supplementary material associated with this article can be found, in the online version, at doi:10.1016/j.cclet.2022.03.060.

References

[1] F. Jiao, B. Xu, Adv. Mater. 31 (2019) 1805173.
[2] T. Xu, B.Y. Ma, J. Liang, et al., Acta Phys. Chim. Sin. 37 (2021) 2009043.
[3] M.M. Shi, D. Bao, S.J. Li, et al., Adv. Energy Mater. 8 (2018) 1800124.
[4] B. Hu, M.W. Hu, L. Seefeldt, T.L. Liu, ACS Energy Lett. 4 (2019) 1053–1054.
[5] S.Z. Andersen, V. Olić, S. Yang, et al., Nature 570 (2019) 504–508.
[6] D.R. Macfarlane, P.V. Cherepanov, J. Choi, et al., Joule 4 (2020) 1186–1205.
[7] Y.Q. Liu, L. Huang, Y.X. Fang, X.Y. Zhu, S.J. Dong, Nano Res. 14 (2021) 2711–2716.
[8] X.W. Zhai, H.X. Yan, G.X. Ge, et al., Appl. Surf. Sci. 506 (2020) 144941.
[9] X.W. Guo, S.M. Chen, H.J. Wang, et al., J. Mater. Chem. A 7 (2019) 19831–19837.
[10] J.R. Han, Z.C. Liu, Y.J. Ma, et al., Nano Energy 52 (2018) 264–270.
[11] W.K. Wang, S.B. Zhang, Y.Y. Liu, et al., Chin. Chem. Lett. 32 (2021) 805–810 32.
[12] W.C. Xu, G.L. Fan, J.L. Chen, et al., Angew. Chem. Int. Ed. 59 (2020) 3511–3516.
[13] N. Zhang, A. Jalil, D.X. Wu, et al., J. Am. Chem. Soc. 140 (2018) 9434–9443.
[14] X.W. Lv, X.L. Liu, Y.J. Suo, Y.P. Liu, Z.Y. Yuan, ACS Nano 15 (2021) 12109–12118.
[15] J.J. Wang, M.Y. Shi, G.L. Yi, et al., Chin. Chem. Lett. 33 (2022) 4623–4627.
[16] W.B. Qiu, X.Y. Xie, J.D. Qiu, et al., Nat. Commun. 9 (2018) 3485.
[17] Y.X. Zhao, F. Wu, Y.X. Miao, et al., Angew. Chem. Int. Ed. 60 (2021) 21728–21731.
[18] J.L. Qu, J.W. Xiao, H.T. Chen, et al., Chin. J. Catal. 42 (2021) 288–296.
[19] B. Huang, Y.F. Wu, B.B. Chen, et al., Chin. J. Catal. 42 (2021) 1160–1167.
[20] L.L. Han, M.C. Hou, P.F Ou, et al., ACS Catal. 11 (2021) 509–516.
[21] J. Xu, S.H. Lai, D.F. Qi, et al., Nano Res. 14 (2021) 1374–1381.
[22] L. Li, H.J. Chen, L Li, et al., Chin. J. Catal. 42 (2021) 1755–1762.
[23] S. Cheng, Y.J. Gao, Y.L. Yan, et al., J. Energy Chem. 39 (2019) 144–151.
[24] Y.J. Yang, S.Q. Wang, H.M. Wen, et al., Angew. Chem. 131 (2019) 15506–15510.
[25] H.Y.F. Sim, J.R.T. Chen, C.S.L. Koh, et al., Angew. Chem. Int. Ed. 59 (2020) 16997–17003.
[26] H. Zhao, D. Zhang, Z.C. Wang, et al., Appl. Catal. B: Environ. 265 (2019) 118481.
[27] H. Cheng, L.X. Ding, G.F. Chen, et al., Adv. Mater. 30 (2018) 1803694.
[28] C. Chen, D.F. Yan, Y. Wang, et al., Small 15 (2019) 1805029.
[29] S.L. Chen, H. Jang, J. Wang, et al., J. Mater. Chem. A 8 (2020) 2099–2104.
[30] S.X. Li, Y.M. Wu, Q. Liu, et al., Inorg. Chem. Front. 8 (2021) 3105.
[31] H.J. Chen, J. Liang, L. Li, et al., ACS Appl. Mater. Interfaces 13 (2021) 41715–41722.
[32] H.J. Chen, J. Liang, K. Dong, et al., Inorg. Chem. Front. 9 (2022) 1514.
[33] T. Xu, J. Liang, Y.Y. Wang, et al., Nano Res. 15 (2022) 1039–1046.
[34] R.D. Milton, S.D. Minteer, Acc. Chem. Res. 52 (2019) 3351–3360.
[35] J. Kim, D.C. Rees, Science 257 (1992) 1677–1682.
[36] W.R. Liao, L. Qi, Y.L. Wang, et al., Adv. Funct. Mater. 31 (2021) 2009151.
[37] K. Chu, H.F. Nan, Q.Q. Li, et al., J. Energy Chem. 53 (2021) 132–138.
[38] X.L. Xue, R.P. Chen, C.Z. Yan, et al., Nano Res. 12 (2019) 1229–1249.
[39] A.T.B.A. Egill Sku Lason, B.F.A.C. Jan Rossmeisl, J.K. Nørskov, Phys. Chem. Chem. Phys. 14 (2012) 1235–1245.
[40] J. Zhao, J.X. Zhao, Q.H. Cai, Phys. Chem. Chem. Phys. 20 (2018) 9248–9255.
[41] L. Zhang, X.Q. Ji, X. Ren, et al., Adv. Mater. 30 (2018) 1800191.
[42] X.H. Li, T.S. Li, Y.J. Ma, et al., Adv. Energy Mater. 8 (2018) 1801357.
[43] S. Licht, B.C. Cui, B.H. Wang, et al., Science 345 (2014) 637–640.
[44] J.H. Montoya, C. Tsai, A. Vojvodic, J.K. Nøskov, ChemSusChem 8 (2015) 2180–2186.
[45] C.Y. Ling, Y.X. Ouyang, Q. Li, et al., Small Methods 3 (2018) 1800376.
[46] T.W. He, S. Matta, A.J. Du, Phys. Chem. Chem. Phys. 21 (2019) 1546–1551.
[47] D.D. Han, X.J. Liu, J.Y. Cai, et al., J. Energy Chem. 59 (2021) 55–62.
[48] Y.W. Peng, C.S. Shan, H.J. Wang, et al., Adv. Energy Mater. 9 (2019) 1900597.
[49] S.S. Wang, G.Y. Yang, Chem. Rev. 115 (2015) 4893–4962.
[50] K.A. Brown, D.F. Harris, M.B. Wilker, et al., Science 352 (2016) 448–450.
[51] Y. Ling, F.M.D. Kazim, S.X. Ma, et al., J. Mater. Chem. A 8 (2020) 12996–13003.
[52] J.X. Zhao, Z.F. Chen, J. Am. Chem. Soc. 139 (2017) 12480–12487.
[53] S.M. Islam, A.S. Roy, R.C. Dey, S. Paul, J. Mol. Catal. A: Chem. 394 (2014) 66–73.
[54] H.J. Yan, Y. Xie, Y.Q. Jiao, et al., Adv. Mater. 30 (2018) 1704156.
[55] Y. Yang, Y.M. Qian, H.J. Li, et al., Sci. Adv. 6 (2020) a6586.
[56] R. Wang, G.F. Zhang, H.X. Zhao, Catal. Today 149 (2010) 117–121.
[57] G.W. Watt, J.D. Chrisp, Anal. Chem 24 (1952) 2006–2008.